3D Optical Flow Estimation in Cardiac CT Images using the Hermite transform

Ernesto Moya-Albor[a], Carlos Mira[b], Jorge Brieva[a],
Boris Escalante-Ramírez[b] and Enrique Vallejo Venegas[c];

[a] Universidad Panamericana. Campus México. Facultad de Ingeniería.
Augusto Rodin 498, México, Ciudad de México, 03920, México.
[b] Fac. de Ingeniería, Universidad Nacional Autónoma de México, Ciudad de México.
[c] Hospital Ángeles del Pedregal, Ciudad de México.

ABSTRACT

Heart diseases are one of the most important causes of death in the Western world. It is, then, important to implement algorithms to aid the specialist in analyzing the heart motion. We propose a new strategy to estimate the cardiac motion through a 3D optical flow differential technique that uses the Steered Hermite transform (SHT). SHT is a tool that performs a decomposition of the images in a base that model the visual patterns used by the human vision system (HSV) for processing the information. The $3D + t$ analysis allows to describe most of motions of the heart, for example, the twisting motion that takes place on every beat cycle and to identify abnormalities of the heart walls. Our proposal was tested on two phantoms and on two sequences of cardiac CT images corresponding to two different patients. We evaluate our method using a reconstruction schema, for this, the resulting 3D optical flow was applied over the volume at time t to obtain a estimated volume at time $t + 1$. We compared our 3D optical flow approach to the classical Horn and Shunk's 3D algorithm for different levels of noise.

Keywords: Optical flow, Differential method, Steered Hermite transform, Cardiac CT imaging, 3D sequences.

1. INTRODUCTION

Heart failure is a major health problem in developed countries and growing in developing countries.[1] Some heart diseases as myocardial infarction, ischemia or hypertrophy can be characterized by analyzing the dynamics of the heart. During the cardiac cycle, contraction (systole) and relaxation (diastole) of the heart, the motion wall estimation can be used to recognize those pathologies.

Different techniques of medical imaging are used commonly to analyze the heart. Cardiac CT is one of the most important method due to its good temporal resolution and its possibility to provide images through different planes or three-dimensional images of the body.[2] It is then possible to acquire good quality cardiac CT data of the heartbeats. Images are acquired over all cardiac cycles to produce the final volume image. It is still hard for the physician to estimate the 3D motion during the exam. Therefore, it is important to develop new algorithms to estimate 3D motion. Several methods have been used to estimate the optical flow of the endocardial wall motion.[3] Research on the measurement of cardiac motion has been commonly made in $2D + t$[4] but this analysis should be done in $3D + t$ to enable us to describe the true motions of the heart, for example, the twisting motion that takes place on every beat cycle. Compared to the 2D analysis, the 3D analysis has not received such attention, although there are currently working groups that analyze optical flow in 3D mainly using ultrasound images.[5–8]

Send correspondence to E.M.A.
E.M.A.: emoya@up.edu.mx, Telephone: +52 55 5482 1600 Ext. 5210
C.M: miragnlz@live.com,
J.B.: jbrieva@up.edu.mx,
B.E.R.: boris@servidor.unam.mx,
E.V.V.: vallejo.enrique@gmail.com

12th International Symposium on Medical Information Processing and Analysis, edited by Eduardo Romero, Natasha Lepore, Jorge Brieva, Ignacio Larrabide, Proc. of SPIE Vol. 10160, 1016010
 · doi: 10.1117/12.2256777

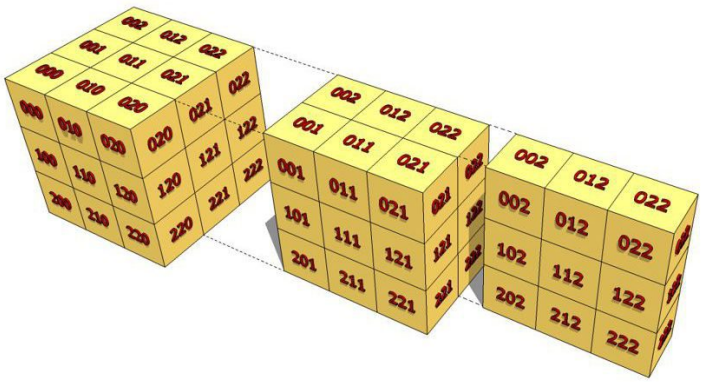

Figure 1. Distribution of the 3D Cartesian Hermite coefficients of a second-order voxel.

We propose a differential method for estimating the three-dimensional optical flow using the 3D Steered Hermite transform, which is inspired by the human vision system (HVS).[9] This model mimics some of the more important properties of early vision such as local processing and the Gaussian derivative models of receptive fields.[10–12] A rotated version of the Hermite transform provides a very efficient representation of oriented patterns which enables an adaptation to local orientation content at each window position over the image, indicating the direction of two-dimensional pattern.

Our approach is a extrapolation to three dimensions of the well known Horn and Schunck's method[13] combined with the 2D optical flow based on the Hermite transform proposed by Moya et al.[14] The rest of the paper is organized as follows: Section 2 describes the 3D Hermite Transform, Section 3 presents the experimental results and discussion of this work, finally Section 4 concludes the paper and presents future work.

1.1 The 3D Hermite Transform

The Hermite transform (HT) is a perceptual model that decomposes digital images in relevant visual features. It uses an approach that emulate the behavior of some important processes present in the human vision system (HVS), as the use of a overlapping of Gaussian functions and the use of Gaussian derivative operators that are found in the receptive fields of the HVS.[9,15,16]

The 3D Hermite transform is a three-dimensional case of the original definition of Martens,[11,12] where the 3D Cartesian Hermite coefficients $L_{l,m-l,n-m}$ are obtained by the convolution of the original signal $L(x,y,z)$ with the analysis filters $D_l(x)$, $D_{m-l}(y)$ and $D_{n-m}(z)$ followed by a subsampling on a three-dimensional mesh S by means of Eq. (1):

$$L_{l,m-l,n-m}(x_0,y_0,z_0) = L(x,y,z) \otimes D_{l,m-l,n-m}(x,y,z), \tag{1}$$

where $L_{l,m-l,n-m}(x,y,z)$ are the 3D Cartesian Hermite coefficients; l, $(m-l)$ and $(n-m)$ denote the analysis order in x, y and z direction, respectively; $n = 0,1,\ldots,N$; $l,m = 0,1,\cdots,n$; N is the maximum order of the expansion that is related with the size of the window of $\mathcal{M}\times\mathcal{M}$ as $N \leq 2*(\mathcal{M}-1)$.

Fig. 1 shows the three-dimensional distribution of the 3D Cartesian Hermite coefficients of order two ($N=2$) in each direction, in this case 27 coefficients are obtained for each voxel of a volume.

The Hermite filters $D_{l,m-l,n-m}(x,y,z)$ are determined by a Gaussian window $v^2(x,y,z)$ that expands the local information in terms of a family of polynomials $G_{l,m-l,n-m}(x,y,z)$ that are orthogonal with respect to the Gaussian window. The analysis filters $D_{l,m-l,n-m}(x,y,z) = D_l(x)D_{m-l}(y)D_{n-m}(z)$ have the separability property by the symmetry of the Gaussian window and they can be obtained by Eq. (2):

$$D_k(x) = \frac{(-1)^k}{\sqrt{2^k k!}} \frac{1}{\sigma\sqrt{\pi}} H_k\left(\frac{x}{\sigma}\right) \exp\left(-\frac{x^2}{\sigma^2}\right), \tag{2}$$

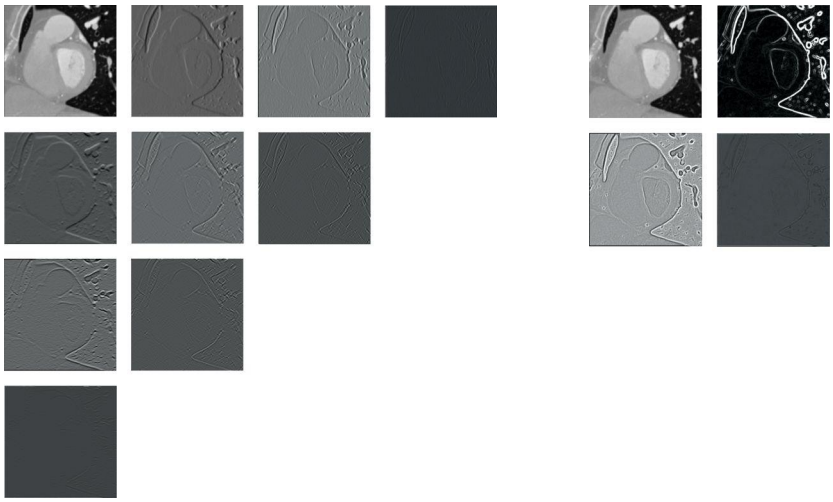

(a) The 2D Hermite coefficients $N = 3$ $\begin{bmatrix} L_{0,0} & L_{1,0} & L_{2,0} & L_{3,0} \\ L_{0,1} & L_{1,1} & L_{2,1} & \\ L_{0,2} & L_{1,2} & & \\ L_{0,3} & & & \end{bmatrix}$

(b) The 2D steered Hermite coefficients $N = 3$ $\begin{bmatrix} L_{0,0} & l_{1,\theta} \\ l_{2,\theta} & l_{3,\theta} \end{bmatrix}$

Figure 2. The Hermite coefficients of a cardiac CT image.

where H_n represents the generalized Hermite polynomials (Eq. 3) and $k = 0, 1, 2, \ldots, \infty$.

$$H_n\left(\frac{x}{\sigma}\right) = (-1)^n \exp\left(-\frac{x^2}{\sigma^2}\right) \frac{d^n}{dx^n} \exp\left(-\frac{x^2}{\sigma^2}\right). \tag{3}$$

A steered version of Hermite transform called the Steered Hermite transform (SHT)[17] is obtained by projecting the 3D Cartesian Hermite coefficients towards two local orientation angles (θ and ϕ) by Eq. (4):

$$l_{l,m-l,n-m,\theta,\phi}(x_0, y_0, z_0) = \sum_{m=0}^{n} \sum_{l=0}^{m} \left(L_{l,m-l,n-m}\left(x_0, y_0, z_0\right) \cdot g_{l,m-l}\left(\theta\right) \cdot g_{m,n-m}\left(\phi\right)\right), \tag{4}$$

where $l_{l,m-l,n-m,\theta,\phi}(x_0, y_0, z_0)$ are the 3D Steered Hermite coefficients.

To illustrate the results of the Hermite transform, in Fig. 2 (left) we show the Hermite coefficients (the cartesian coefficients) for a cardiac CT image where $N = 3$ ($l = 0, 1, \ldots, N$, $m = 0, 1, \cdots, l$ and $n = 0$, i.e., case 2D). In Fig. 2 (right) we show the steered Hermite coefficients for the Cartesian Hermite coefficients of Fig. 2 (left).

Fig. 3 shows the 3D Cartesian and the Steered Hermite coefficients on a volume representing the change of the reference system and the approximation of θ and ϕ angles according to the gradient direction.

To calculate the direction of maximum energy we used the phase of the gradient given by Eq. (5):

$$\begin{aligned} \theta &= \arctan \frac{L_{010}}{L_{100}}, \\ \phi &= \arctan \frac{\sqrt{\left(L_{100}\right)^2 + \left(L_{010}\right)^2}}{L_{001}} \end{aligned} \tag{5}$$

where $\left[L_{1,0,0}, L_{0,1,0}, L_{0,0,1}\right](x, y, z)^\top$ is a good approximation of the 3D gradient through the Cartesian Hermite coefficients.

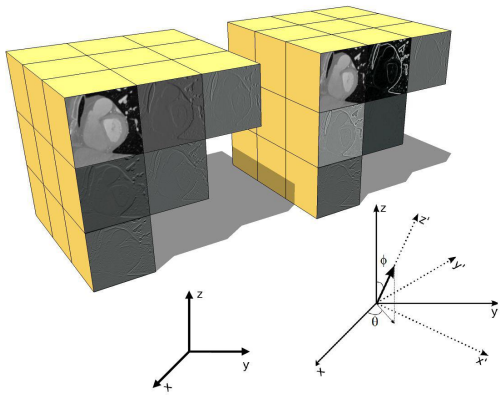

Figure 3. Ensemble of the 3D Cartesian (left) and Steered (right) Hermite coefficients of a cardiac CT volume.

2. OPTICAL FLOW USING THE HERMITE TRANSFORM

A differential method based on the work by Horn and Schunck (HS)[13] was used to calculate the optical flow method and, in order to avoid the main disadvantage of this method (low accuracy), the 3D Hermite transform was proposed as a biological visual model. The local constraints of Horn and Schunck approach are defined using the zero order and the 3D Steered Hermite coefficients as local descriptors of visual features of the volumes.

2.1 Model

The modified version of Horn and Shunck approach that allows to increase the accuracy of the optical flow by using the Hermite transform, which involves an expansion of the Constant Intensity Constraint with the incorporation of the 3D Steered Hermite Coefficient Constraint, is defined as follows:

$$\left[L_0\left(\mathbf{x}+\mathbf{w}\right)-L_0\left(\mathbf{x}\right)\right]+\gamma\left[\sum_{n=1}^{N} l_{n,\theta,\phi}\left(\mathbf{x}+\mathbf{w}\right)-\sum_{n=1}^{N} l_{n,\theta,\phi}\left(\mathbf{x}\right)\right]=0, \tag{6}$$

where $L\left(\mathbf{x},t\right)$ is a volume sequence, with $\mathbf{x}=\left(x,y,z,t\right)^T$ representing the voxel location within a cubic volume domain V; $\mathbf{w}:=\left(u,v,w,1\right)^T$ is a vector that defines the displacement u, v and w for each voxel at position (x,y,z) within the sequence of volumes at a time t to a time $(t+1)$ in the directions x, y and z respectively; and γ is a weight parameter.

Thus, the modified functional of Horn and Schunck[13] can be expressed as given by Eq. (7):

$$\mathrm{E}=\int_V\left(\left[L_0(\mathbf{x})_0-L_0(\mathbf{x}+\mathbf{w}+d\mathbf{w})_1\right]^2+\gamma\left[\sum_{n=1}^{N}\left\{l_{n,\theta,\phi}(\mathbf{x})_0-l_{n,\theta,\phi}(\mathbf{x}+\mathbf{w}+d\mathbf{w})_1\right\}\right]^2+\alpha|\nabla\left(\mathbf{w}+d\mathbf{w}\right)|^2\right)d\mathbf{x}. \tag{7}$$

To simplify the notation $L_{000}\left(\mathbf{x}\right)=L_0\left(\mathbf{x}\right)$. $L_*(\mathbf{x})_*$ is the Cartesian Hermite coefficient $*$ at time t and $L_*(\mathbf{x})_1$ is the Cartesian Hermite coefficient $*$ at time $t+1$.

Considering linear displacements in Eq. (6), by performing an expansion by Taylor series and by simplifying the derivatives of the Hermite coefficients, as was demonstrated in,[14] we obtain the 3D Horn-Hermite optical flow functional (HOF3D) as follows:

$$\begin{aligned}E\left(\mathbf{w}\right)=\int_V\Big(&-\left[L_0(\mathbf{x})_t+du\,L_{100}(\mathbf{x})_W+dv\,L_{010}(\mathbf{x})_W+dw\,L_{001}(\mathbf{x})_W\right]^2\\&-\gamma\sum_{n=1}^{N}\left[l_{n,\theta,\phi}(\mathbf{x})_t+du\;l_{n,\theta,\phi,(m+1)}(\mathbf{x})_W+dv\;l_{n,\theta,\phi,(n+1)}(\mathbf{x})_W+dw\;l_{n,\theta,\phi,(l+1)}(\mathbf{x})_W\right]^2\\&+\alpha|\nabla\left(\mathbf{w}+d\mathbf{w}\right)|^2\Big)\,d\mathbf{x},\end{aligned} \tag{8}$$

where:

$$L_0(\mathbf{x})_t = L_0(\mathbf{x}+\mathbf{w})_1 - L_0(\mathbf{x})_0, \tag{9}$$

$$L_{100}(\mathbf{x}+\mathbf{w}) = L_{100}(\mathbf{x})_W = \frac{\partial L_{000}(\mathbf{x}+\mathbf{w})_1}{\partial x}, \tag{10}$$

$$l_{n,\theta,\phi}(\mathbf{x})_t = l_{n,\theta,\phi}(\mathbf{x})_1 - l_{n,\theta,\phi}(\mathbf{x}+\mathbf{w})_0, \tag{11}$$

and

$$l_{n,\theta,\phi,(m+1)}(\mathbf{x})_W = \frac{\partial l_{n,\theta,\phi}(\mathbf{x}+\mathbf{w})_1}{\partial x}. \tag{12}$$

The functional of Eq. (8) was implemented within a multiresolution approach in order to calculate the small displacements du and dv and to propagate the solution to higher resolution levels. For each resolution level an iterative method for solving linear equations was carried out. Fig. 4 shows the steps of our method.

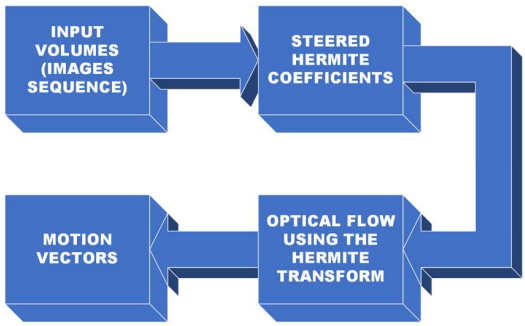

Figure 4. Procedure to implement the HOF3D approach.

3. EXPERIMENTS AND RESULTS

Our data set consists of two sequences of cardiac CT images. The tomographic studies were acquired with a SIEMENS 16-slice CT system at 120kVp of tube voltage and 900mA. The scanner is composed of 128 detectors and is synchronized with the ECG signal. Each image has a size of 512x512 pixels, quantized to 12 bits per pixel. A contrast agent was also applied to each patient. Each sequence is composed by 10 frames showing the heart variation throughout the entire cardiac cycle from diastole to systole.

In this section we present the results of the estimation of optical flow. To conduct the experiments, two synthetic volumes were generated, one of them (a hexahedron) with a lateral displacement and another one (a sphere) with a movement of expansion, were used. Also two sets of volumes, corresponding to medical CT images were considered.

Although the constants, values and weight parameters are difficult to select and they depend on the particular volume sequence, we experimentally found that good estimation of optical flow results for our dataset are achieved with: for the three-dimensional Steered Hermite coefficients $N = 4$, for the multiresolution scheme five levels and for the numerical solution 50 iterations.

For the functional of the Eq. (7), the weight parameter γ is used to weigh the contribution of the high order Hermite coefficients in those regions where the intensity does not remain constant of a volume of another. Secondly, the weight value of the smoothness term α can get information from neighbors in regions where the intensity gradient is zero (uniform regions of flow), using averages from structures with spatial high frequencies (i.e. edges). Large values of α give us a smoother flow but is relatively less important at locations with high image gradients than elsewhere.

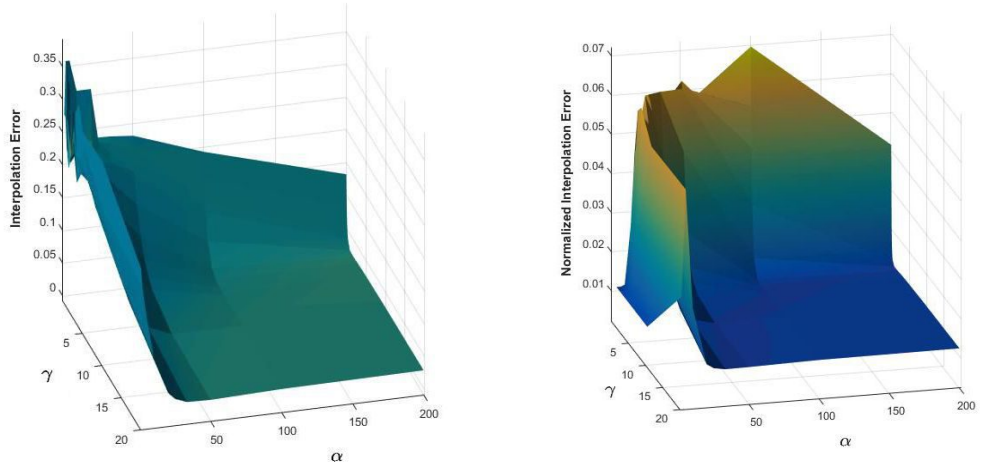

(a) (b)

Figure 5. Interpolation Error (a) and Normalized Interpolation Error (b), from sequences of the cardiac CT volumes.

For determining the values of the smoothness weight α and the weight parameter γ we performed a first experiment over the available sequences of the cardiac CT volumes, we computed the 3D optical flow for several values of α and γ to analyze the behavior of the Interpolation Error (IE) and Normalized Interpolation Error (NE) metrics.

In the case of CT volumes there is not a ground-truth for the optical flow, so a reconstruction between the volume in time t and the optical flow result was performed. The interpolation error is the root-mean-square (RMS) difference between the known volume and the estimated interpolated volume as in:[18,19]

$$IE_{3D} = \left[\frac{1}{M} \sum_{(x,y,z)} \left(I(x,y,z) - I_{GT}\left(x,y,z\right) \right)^2 \right]^{\frac{1}{2}} \tag{13}$$

where M is the number of voxels.

We also compute a second measure of interpolation performance, the normalized interpolation error between an interpolated volume $I(x,y,z)$ and a ground-truth volume $I_{GT}\left(x,y,z\right)$, which is given as in:[20]

$$NE_{3D} = \left[\frac{1}{M} \sum_{(x,y,z)} \frac{\left(I(x,y,z) - I_{GT}\left(x,y,z\right) \right)^2}{\left\| \nabla I_{GT}\left(x,y,z\right) \right\|^2 + \varepsilon} \right]^{\frac{1}{2}} \tag{14}$$

that represents a gradient-normalized RMS error, where ϵ is a scaling constant (e.g., $\epsilon = 1$).

Fig. 5 shows that the best results for IE and NE are from $\alpha = 100$ and $\gamma = 10$ onwards. Both graphics are represented by a three-dimensional mesh being the best values the bottom of that mesh.

We tested the performance of the proposed HOF3D method in a second experiment using one of the synthetic volumes generated (a sphere). We simulated the noisy volume using a pseudorandom number generator with zero mean and different standard deviations (σ_n) which was subsequently added to the original volume. In this experiment σ_n was set to 0, 5, 10, 15, 20 and 30. In Table 1 we show the interpolation error and the normalized interpolation error for the noise levels given for the HOF3D method using optimized parameters $\alpha = 100$, $\gamma = 10$ and $N = 4$. The proposed method has good results in volumes with standard deviations of noise smaller than 30.

Table 1. Interpolation Error and Normalized Interpolation Error computed for a synthetic sphere sequence with several standard deviation σ_n of Gaussian noise.

Gaussian Noise (σ_n)	Interpolation Error	Normalized Interpolation Error
0	0.03384	0.00866
5	0.05044	0.01012
10	0.05447	0.01699
15	0.05813	0.01797
20	0.05936	0.01869
30	0.06707	0.02371

We also present the results of the 3D optical flow for two cardiac CT sequences in Fig. 6. Both sequences were analyzed from 0% to 90% of the cardiac cycle, labeled as 0 (from 0% to 10%), 10 (from 10% to 20%) 20 (from 20% to 30%), and so on. To compare our algorithm we obtained two optical flows, first one from a three-dimensional Horn-Schunck method to compare it with our HOF3D method.

In both sequences we can observe the increment of the interpolation error from 20% to 30% (systole) and from 50% to 60% of the cardiac cycle (diastole), where we have the stronger cardiac movement. Also we can see that our method (HOF3D) give us a better performance in all the cases.

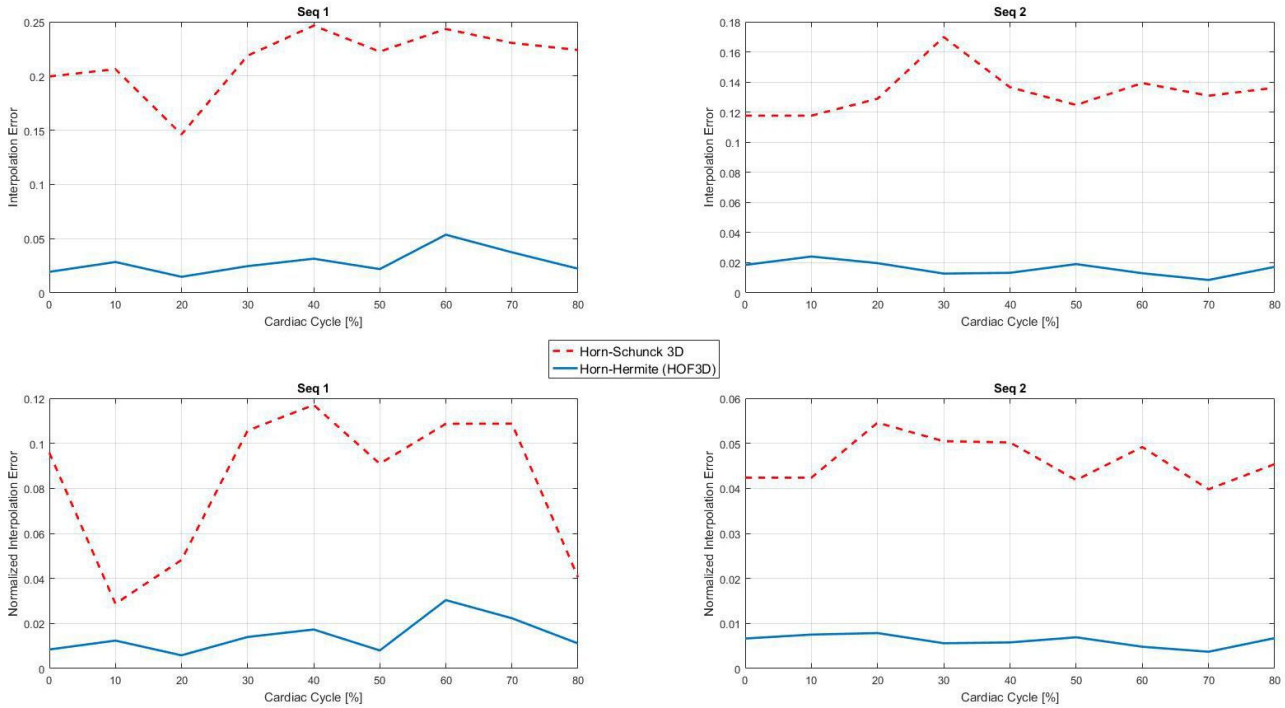

Figure 6. Interpolation Error (red dashed line) and Normalized Interpolation Error (blue solid line) for the 3D Horn-Schunck and HOF3D methods, from two sequences of the cardiac CT volumes.

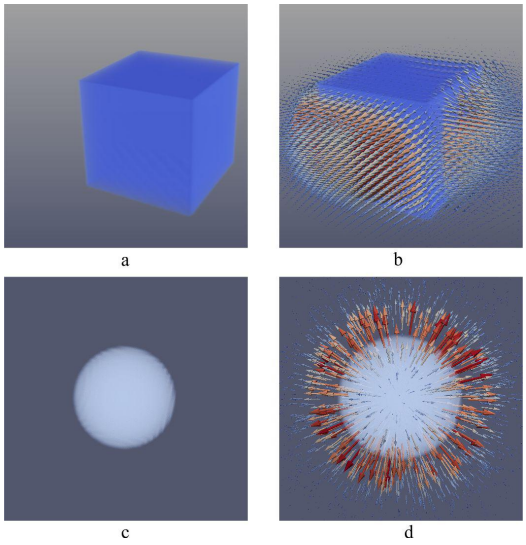

Figure 7. Optical flow of synthetic volumes. A hexahedron (a), a hexahedron displaced laterally and its optical flow (b), a sphere (c) and a sphere expanded and its optical flow (d).

Fig. 7 (a) and (b) shows the optical flow results for a synthetic hexahedron which it's being displaced laterally. In Fig. 7(a) the hexahedron in the first position is shown and in Fig. 7(b) the resulting flow is shown as well as the displaced hexahedron which coincides with the hexahedron extrapolated from the first volume and flow obtained. In Fig. 7 (c) and (d) we show a synthetic sphere expanding. In Fig. 7(c), the sphere is in its first stage, Fig. 7(d) the sphere is expanded and the resulting flow is shown along with the interpolated sphere through the flow.

In Fig. 8 we show a cardiac CT volume at 30% and 60% of the cardiac cycle. In both cases we can observe the original volume (left), the interpolated volume (center), the difference between the original (ground-truth) volume and its interpolated result (right).

In Fig. 9 we can see the results of a 3D Optical flow of two cardiac CT volumes computed at phases 20-30% using the HOF3D method. The top image shows two phases of the cardiac cycle of volume 1 (for better viewing a cut that volume was made). The bottom of the image shows the same phases of volume along with the three-dimensional optical flow field.

4. CONCLUSIONS

In this paper we proposed a method for estimating the optical flow made entirely in 3D because this kind of analysis enables us to describe most of the true motions of the heart, for example, the twisting motion that takes place on every beat cycle.

Our approach for motion estimation have included a differential algorithm well known as Horn-Schunck method and image structure information extracted from the Steered Hermite coefficients in the constraint terms of the minimizing function. The Steered Hermite transform is a model that incorporates some important properties of the first stages of the human visual system, such as the overlapping Gaussian receptive fields, the Gaussian derivative model of early vision,[10] and a multiresolution analysis.[21,22] One of the advantages of this approach is that the spatial scale of analysis becomes a free parameter that can be adjusted to make the algorithm more robust to noise or to analyze spatial objects of different spatial dimensions. Another advantage is the inclusion of structures obtained from higher order Gaussian derivatives which improves the estimation performance.

The proposed framework was validated first with several sequences of cardiac CT images and compared with Horn-Schunck method and then with synthetic volumes. The results were evaluated for each volume of the sequences using a couple of metrics. We obtained experimentally the optimum values for subsequent tests.

Regarding cardiac testing volumes, we observed that the interpolation errors were increasing as we approach the systolic phase (between 20% and 30%) where there is a faster movement. To some degree, that happens to the relaxation movement (between 50% and 60%) but with a lower error. We could also observe that the use of our method (HOF3D) generally get lower interpolation errors and minor variations than with a traditional method.

Our proposal in which we can visualize the 3-dimensional vector field is a promising technique to better describe the dynamics of cardiac cycles and the detection of some possible disease. Because the heart is an organ that occupies a three-dimensional space, it is best to analyze and evaluate it in 3D. As future work we can identity and characterize the main patterns of the heart movement using our 3D optical flow approach.

ACKNOWLEDGEMENTS

Ernesto Moya-Albor and Jorge Brieva would like to thank the Facultad de Ingeniería of Universidad Panamericana for all support in this work.

Carlos Mira gratefully acknowledges the scholarship from CONACyT to pursue his doctoral studies.

Boris Escalante-Ramírez gives a special thank to UNAM grant PAPIIT IG100814.

REFERENCES

[1] Cheung, Y. f., "The role of 3d wall motion tracking in heart failure," *Nature Reviews Cardiology* **9**, 644(14) (2012).

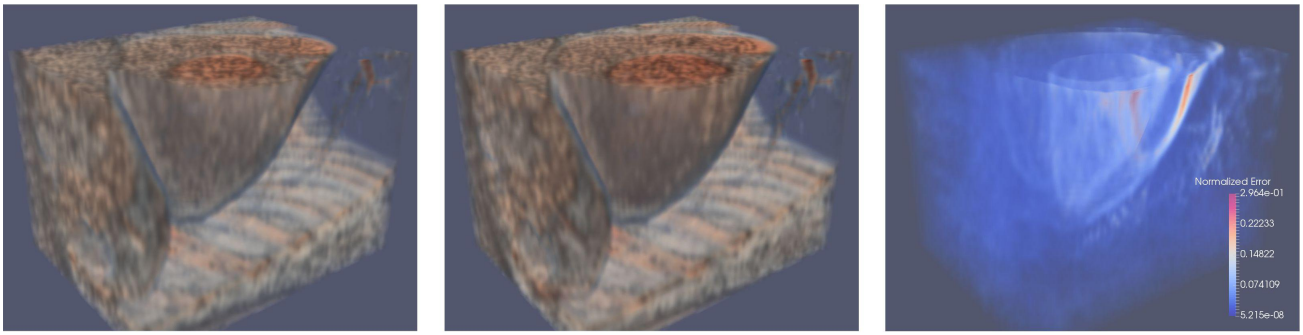

Volume at 30% (ground-truth) | Volume at 30% (interpolated) | Difference between ground-truth and interpolated volumes

(a)

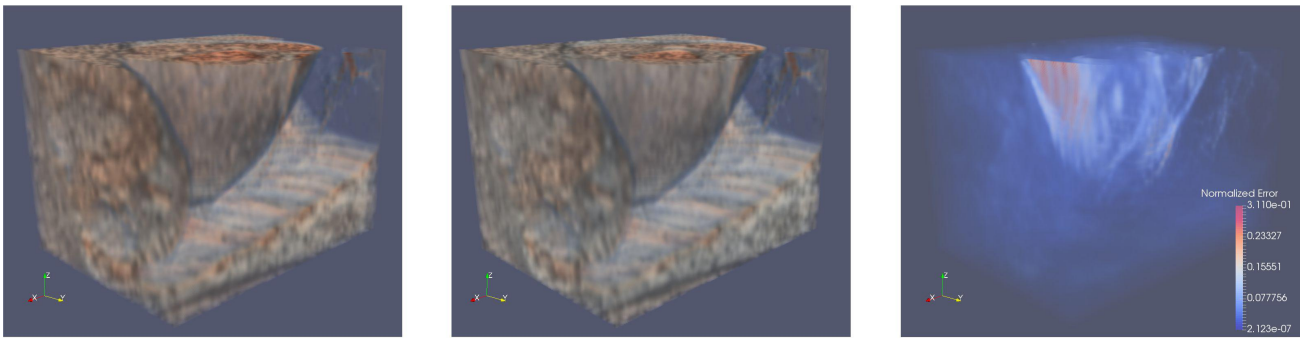

Volume at 60% (ground-truth) | Volume at 60% (interpolated) | Difference between ground-truth and interpolated volumes

(b)

Figure 8. A cardiac CT volume at 30% (a) and 60% (b) of the cardiac cycle. The original volume (left), the interpolated volume (center), the difference between the original (ground-truth) volume and its interpolated result (right).

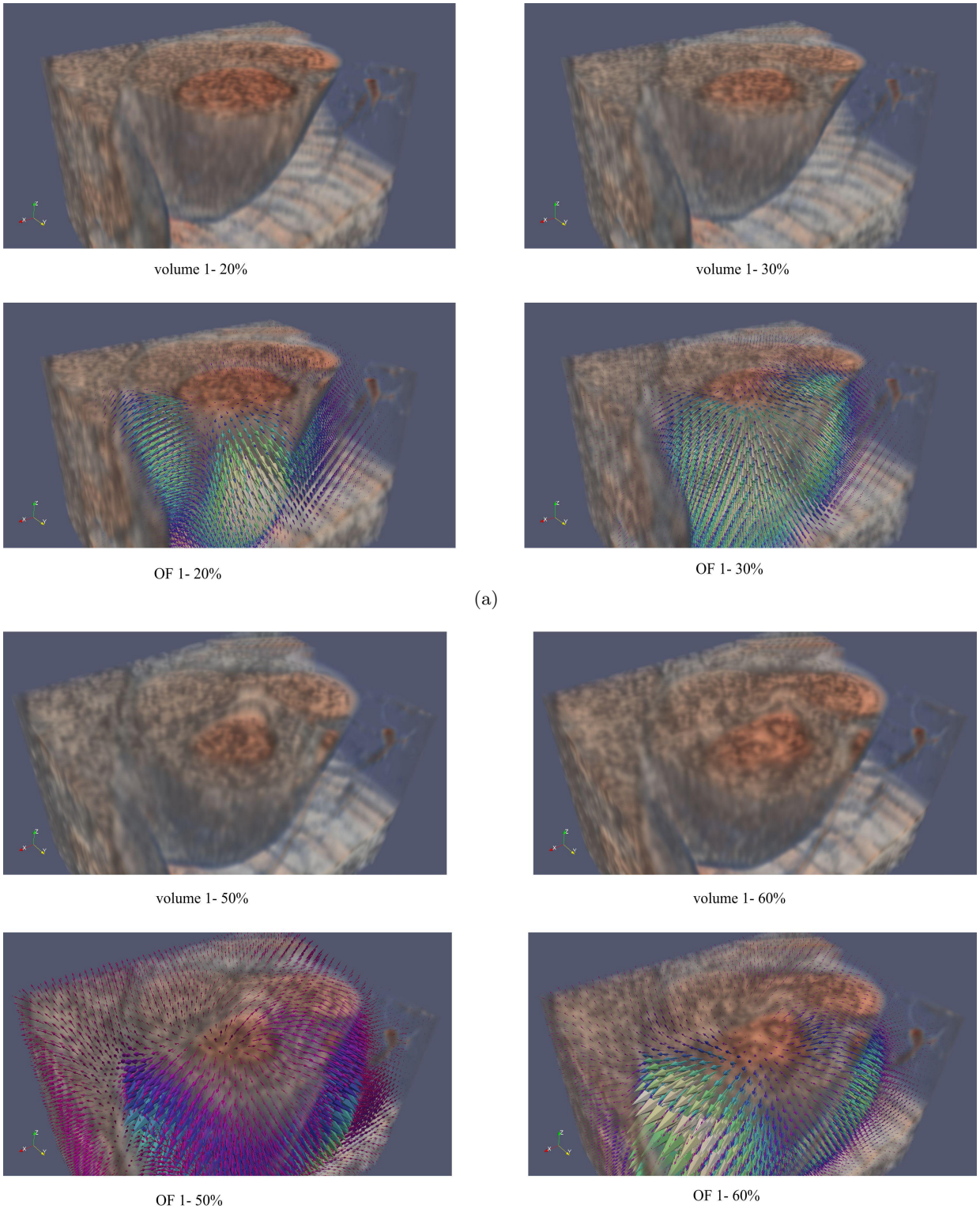

Figure 9. Results of 3D Optical flow of two cardiac CT volumes computed at phases 20-30% (a) and 50%-60% (b) using the HOF3D method.

[2] Schoenhagen, P., Stillman, A., Halliburton, S., and White, R., "Ct of the heart: principles, advances, clinical uses," *Cleveland Clinic Journal of Medicine* **72**(3), 127–140 (2005).

[3] Gorce, J., Friboulet, D., and Magnin, I., "Estimation of three-dimensional cardiac velocity fields : Assessment of a differential method and application to 3D CT data," *Med Image Anal* **1**(3), 127–140 (1997).

[4] Barba-J, L., Moya-Albor, E., Escalante-Ramírez, B., Brieva, J., and Venegas, E. V., "Segmentation and optical flow estimation in cardiac CT sequences based on a spatiotemporal PDM with a correction scheme and the Hermite transform," *Computers in Biology and Medicine* **69**, 189 – 202 (2016).

[5] Duan, Q., Angelini, E., Homma, S., and Laine, A., "Validation of optical-flow for quantification of myocardial deformations on simulated RT3D ultrasound," in [*2007 4th IEEE International Symposium on Biomedical Imaging: From Nano to Macro*], 944–947 (April 2007).

[6] Leung, K. Y. E., Danilouchkine, M. G., van Stralen, M., de Jong, N., van der Steen, A. F. W., and Bosch, J. G., "Tracking left ventricular borders in 3d echocardiographic sequences using motion-guided optical flow," *Proc. SPIE* **7259**, 72590W–72590W–12 (2009).

[7] Heyde, B., Cygan, S., Choi, H. F., Lesniak-Plewinska, B., Barbosa, D., Elen, A., Claus, P., Loeckx, D., Kaluzynski, K., and D'hooge, J., "Regional cardiac motion and strain estimation in three-dimensional echocardiography: a validation study in thick-walled univentricular phantoms," *IEEE Transactions on Ultrasonics, Ferroelectrics, and Frequency Control* **59**, 668–682 (April 2012).

[8] Duan, Q., Angelini, E. D., Herz, S. L., Ingrassia, C. M., Gerard, O., Costa, K. D., Holmes, J. W., and Laine, A. F., "Evaluation of optical flow algorithms for tracking endocardial surfaces on three-dimensional ultrasound data," *Proc. SPIE* **5750**, 159–169 (2005).

[9] Sakitt, B. and Barlow, H., "A Model for the Economical Encoding of the Visual Image in Cerebral Cortex," *Biological Cybernetics* **43**(2), 97–108 (1982).

[10] Young, R., [*The Gaussian Derivative Theory of Spatial Vision: Analysis of Cortical Cell Receptive Field Line-weighting Profiles*], Research publication, General Motors Research Laboratories (1985).

[11] Martens, J.-B., "The Hermite Transform-Theory," *IEEE Transactions on Acoustics, Speech and Signal Processing* **38**(9), 1595–1606 (1990).

[12] Martens, J.-B., "The Hermite Transform-Applications," *IEEE Transactions on Acoustics, Speech and Signal Processing* **38**(9), 1607–1618 (1990).

[13] Horn, B. K. P. and Schunck, B. G., "Determining optical flow," *Artificial Intelligence* **17**, 185–203 (1981).

[14] Moya-Albor, E., Escalante-Ramírez, B., and Vallejo, E., "Optical flow estimation in cardiac CT images using the steered Hermite transform," *Signal Processing: Image Communication* **28**, 267–291 (Mar. 2013).

[15] Marr, D. and Hildreth, E., "A theory of edge detection," in [*The Royal Society of London*], *B* **207**(1167), 187–217 (1980).

[16] Bloom, J. and Reed, T., "A gaussian derivative-based transform," *IEEE Transactions on Image Processing* **5**, 551–553 (mar 1996).

[17] Van Dijk, A. M. and Martens, J., "Image representation and compression with steered Hermite transforms," *Signal Processing* **56**(1), 1–16 (1997).

[18] Fleet, D. J. and Jepson, A. D., "Computation of component image velocity from local phase information," *International Journal of Computer Vision* **5**(1), 77–104 (1990).

[19] Barron, J. L., Fleet, D. J., Beauchemin, S. S., and Burkitt, T. A., "Performance of optical flow techniques," in [*Computer Vision and Pattern Recognition, 1992. Proceedings CVPR '92., 1992 IEEE Computer Society Conference on*], 236–242 (Jun 1992).

[20] Otte, M. and Nagel, H. H., [*Optical flow estimation: Advances and comparisons*], 49–60, Springer Berlin Heidelberg, Berlin, Heidelberg (1994).

[21] Escalante-Ramírez, B. and Silván-Cárdenas, J. L., "Advanced modeling of visual information processing: A multiresolution directional-oriented image transform based on Gaussian derivatives," *Signal Processing: Image Communication* **20**(9-10), 801–812 (2005).

[22] Silván-Cárdenas, J. L. and Escalante-Ramírez, B., "The multiscale hermite transform for local orientation analysis," *IEEE Transactions on Image Processing* **15**(5), 1236–1253 (2006).